

Article

Mechanism Analysis of Surrounding Rock Mass Failure Induced by the Multi-Cavern Effect in a Large-Scale Underground Powerhouse

Meng Wang ¹, An-Chi Shi ², Hai-Bo Li ¹, Hong-Chuan Yan ¹, Gang Fan ³ and Jia-Wen Zhou ^{1,*}

¹ State Key Laboratory of Hydraulics and Mountain River Engineering, Sichuan University, Chengdu 610065, China

² PowerChina Huadong Engineering Corporation Limited, Hangzhou 311122, China

³ College of Water Resource and Hydropower, Sichuan University, Chengdu 610065, China

* Correspondence: jwzhou@scu.edu.cn

Featured Application: The research results help to reveal the failure mechanism in the case and to gain a better and actual understanding of the multi-cavern effect. These results have been applied to the dynamic construction and support optimization of the Baihetan underground powerhouse and are expected to provide reference for the stability control of surrounding rock mass in similar underground powerhouses.

Abstract: The underground powerhouse of a hydropower station, in the form of a cavern group, is generally characterized by a large scale and complicated spatial structure. During the construction phase, extensive excavation in limited underground space may cause a multi-cavern effect between adjacent caverns and thus lead to deformation and failure of the surrounding rock mass, which undoubtedly compromises cavern stability and construction safety. This paper takes the drainage gallery LPL5-1 in the Baihetan underground powerhouse (adjacent to the main powerhouse) as a case study. During the excavation of the main powerhouse, the shotcrete at the upstream arch of LPL5-1 cracked, ballooned and peeled off. After field investigation and numerical simulations, the stress evolution induced by excavation is studied and the failure mechanism is analyzed. The results indicate that the multi-cavern effect led to the surrounding rock mass failures in LPL5-1, which is related to the continuous excavation of the main powerhouse and the resultant extensive stress adjustment. During the main powerhouse excavation, a stress concentration zone was generated at the upstream arch and was intensified with the excavation progressed. The expanded stress concentration zone affected LPL5-1 and made its surrounding rock mass split, thus causing the shotcrete cracking.

Keywords: underground powerhouse; rock mass failure; multi-cavern effect; shotcrete crack; high geostress



Citation: Wang, M.; Shi, A.-C.; Li, H.-B.; Yan, H.-C.; Fan, G.; Zhou, J.-W. Mechanism Analysis of Surrounding Rock Mass Failure Induced by the Multi-Cavern Effect in a Large-Scale Underground Powerhouse. *Appl. Sci.* **2023**, *13*, 4376. <https://doi.org/10.3390/app13074376>

Academic Editors: Rongzhu Liang and Cungang Lin

Received: 8 March 2023

Revised: 23 March 2023

Accepted: 28 March 2023

Published: 30 March 2023



Copyright: © 2023 by the authors. Licensee MDPI, Basel, Switzerland. This article is an open access article distributed under the terms and conditions of the Creative Commons Attribution (CC BY) license (<https://creativecommons.org/licenses/by/4.0/>).

1. Introduction

In order to meet the challenges of climate change and energy demand, many large hydropower stations have been under construction or put into operation in southwest China, which has nearly 60% of the waterpower resources of the country. Due to the limit of topography, underground powerhouse structures are usually utilized in these hydropower stations in the form of cavern groups inside bank slopes. These underground powerhouses are generally on a large scale and contain many different kinds of caverns and tunnels. As an underground powerhouse is the key structure of a hydropower station, its safety and surrounding rock mass stability are crucial. Subjected to the high in situ stress and complex geology in the mountainous area in southwest China, many deformation and failure issues of surrounding rock mass arise during the construction of underground powerhouses, such

as rockburst, spalling, splitting, large deformation and collapse [1,2]. These failures and hazards not only threaten the safety of constructors and facilities but also cause economic losses in dealing with them. Therefore, the deformation and failure of surrounding rock mass is a key technical problem in the construction of underground powerhouse to which attention is always paid.

Since the powerhouse is an engineering structure built underground, the properties of the surrounding rock mass are of considerable significance regarding the safety and stability of the underground powerhouse, which is mainly reflected in the strength and structure of the rock mass. On one hand, the underground powerhouse with a large burial depth is usually subjected to high in situ stress; thus, the surrounding rock mass has relatively low strength after excavation. In such circumstances, the contradiction between in situ stress and rock mass strength becomes prominent and high stress can lead to the failure and large deformation of the surrounding rock mass. On the other hand, the geological structure in the rock mass provides a requisite for the deformation and failure. For example, under the combined cutting of structural planes, the surrounding rock mass is likely to collapse after cavern excavation. Thus, the characteristics, mechanisms and countermeasures of the surrounding rock mass deformation and failure are critical technical problems with respect to rock mechanics in the underground engineering field.

On the deformation, failure and stability of the surrounding rock mass, extensive research works have been performed at home and abroad and many valuable and meaningful results have been achieved. Ding et al. [3] analyzed the deformation and cracking characteristics of the surrounding rock mass in the Wudongde underground powerhouse and proposed an optimized support scheme. The results of numerical simulation based on a constitutive model for a layered rock mass provided reference for the support design. Zhou et al. [4] investigated four mechanisms of deformation and failure of steeply dipping layered surrounding rock mass, including unstable rock blocks, failure on the upstream sidewall, shotcrete cracking at the downstream roof and structurally controlled failure on the central pier. Based on in situ microseismic (MS) monitoring experiments, Xiao et al. [5] analyzed the macro-failure characteristics, micro-failure modes and micro-seismicity of a stress-structure controlled collapse and explained its evolution mechanism. With the methods of MS monitoring, conventional monitoring and a three-dimensional distinct element code (3DEC), Hu et al. [6] studied the effect of discontinuities and dynamic construction on the failure mechanism of surrounding rock mass and conducted a stability analysis of an underground powerhouse in a high geostress environment. Wang et al. [7] investigated the failure mechanism of blocks in the collapse area of a tunnel by adopting a method of discontinuities' automatic identification and stability analysis based on terrestrial laser scanning. In regard to the rockburst hazard under high in situ stress, Liu et al. [8] predicted an intense rockburst and identified the location at a deep-buried tunnel with complex geological structures by employing a MS monitoring system. Xue et al. [9] predicted rockburst in an underground powerhouse with a new method based on the rough set theory and the extension theory.

With respect to the stability assessment of surrounding rock mass, Wang et al. [10] presented a practical flowchart of rock mechanics modeling for the steps in the evaluation process of an underground powerhouse. Based on the flowchart, stability analysis using the distinct element method (DEM) was conducted on three underground powerhouses. Kumar et al. [11] conducted a dynamic stability evaluation against the excavation-induced stress adjustment on a large underground powerhouse and identified potential risk zones. Li et al. [12] proposed a novel dynamic method for the stability evaluation of sidewall subjected to flexural toppling, which integrates stability criterion, continuum modeling and MS data. Ren et al. [13] established a comprehensive safety evaluation method of surrounding rock mass, which combines a deformation stability prediction and evaluation method, a rapid prediction method of collapse and a comprehensive early-warning index system. Zhang et al. [14] developed a novel rock mass displacement back-analysis method

considering the displacement loss and applied it in the caverns of the Jinping II hydropower station and the Taian pumped storage power station.

In these studies, new techniques (including MS monitoring) were employed and a combination of multiple technical methods became a typical feature. According to actual engineering demands, previous research has explained the reasons and mechanisms of deformation and failure phenomena. In addition, the stability of surrounding rock mass in underground powerhouses has been comprehensively assessed via a variety of methods.

Compared with other underground openings, the underground powerhouse of a hydropower station is characterized as large scale with a large span, a high sidewall and complex structures. In terms of excavation dimensions, some underground main powerhouses are more than 200 m long and more than 60 m high and have a span of over 25 m. As for spatial structure, the underground powerhouse has many caverns of different functions and sizes. Large caverns include the main powerhouse, the transformer chamber and the tailrace surge chambers. Relatively small caverns include diversion tunnels, omnibus bar caves, tailrace tunnels and auxiliary caverns, such as construction adits and access tunnels. These characteristics have an impact on the surrounding rock mass stability of an underground powerhouse. When the excavation dimension is large, the long-lasting excavation disturbance can increase the risk of surrounding rock mass deformation and failure. With the number of caverns increasing, a multi-cavern effect is likely to appear when adjacent or intersecting caverns are excavated simultaneously, leading to surrounding rock mass instability. Consequently, the large scale and complex structure gives the underground powerhouse unique surrounding rock mass stability issues, which are relatively rare in other engineering structures such as traffic tunnels.

Among these issues, the deformation and failure induced by the multi-cavern effect is typical. The multi-cavern effect is the interaction between adjacent or intersecting caverns during the construction period. When a cavern is excavated, the stress in rock mass close to the free face is unloaded and the stress within a certain range around the cavern is adjusted. With the adjustment and redistribution of stress, the surrounding rock mass exhibits some mechanical behaviors, including deformation, damage and even failure. If there is a cavern adjacent to this cavern, the excavation, stress adjustment and rock mass responses of the two caverns may affect each other. When the interaction is obvious, the rock mass surrounding the caverns is apt to be damaged or to fail. For the large-scale underground powerhouse built in a limited space, extensive excavation blasting and multi-procedure construction will inevitably increase the possibility of interactions between the caverns, thus leading to deformation and failure.

The deformation and failure of surrounding rock mass induced by the multi-cavern effect in an underground powerhouse can be divided into three types: between large caverns (type LL), between a large cavern and a small cavern (type LS) and between small caverns (type SS). The deformation and failure of a rock pillar between the main powerhouse and the transformer chamber belongs to type LL (Figure 1b). The deformation and failure of a small cavern affected by a large cavern such as the main powerhouse belongs to type LS (Figure 1c). Deformation and failure under the impact of adjacent or intersecting small cavern belongs to type SS (Figure 1d). The underground powerhouse usually has many caverns and a compact layout, and the multi-cavern effect is likely to occur during construction. Importance should be attached to the deformation and failure of surrounding rock mass induced by the multi-cavern effect; its reasons and mechanisms should be studied and explained and countermeasures be put forward to ensure the construction safety and long-term stability of the powerhouse.

However, previous studies have rarely focused on failure issues triggered by the multi-cavern effect; this is a research gap at present. This issue usually arises in the underground powerhouse with a large scale and complex spatial structure, which is different from a single cavern. Few cases have been reported so far and not much attention has been paid to this issue. This issue has occurred in a few projects, while previous studies have rarely conducted in-depth analysis on it. The main patterns, characteristics and mechanisms of

the multi-cavern effect have not been systematically summarized. For the underground powerhouse of a hydropower station or a pumped storage power station, the deformation and failure of surrounding rock mass caused by the multi-cavern effect is likely to be prominent during construction. With the scale and burial depth of underground powerhouse increasing and the geological conditions becoming more complex, the importance of this issue will be further highlighted. Hence the multi-cavern effect in underground powerhouses is of great practical significance and is worth further study.

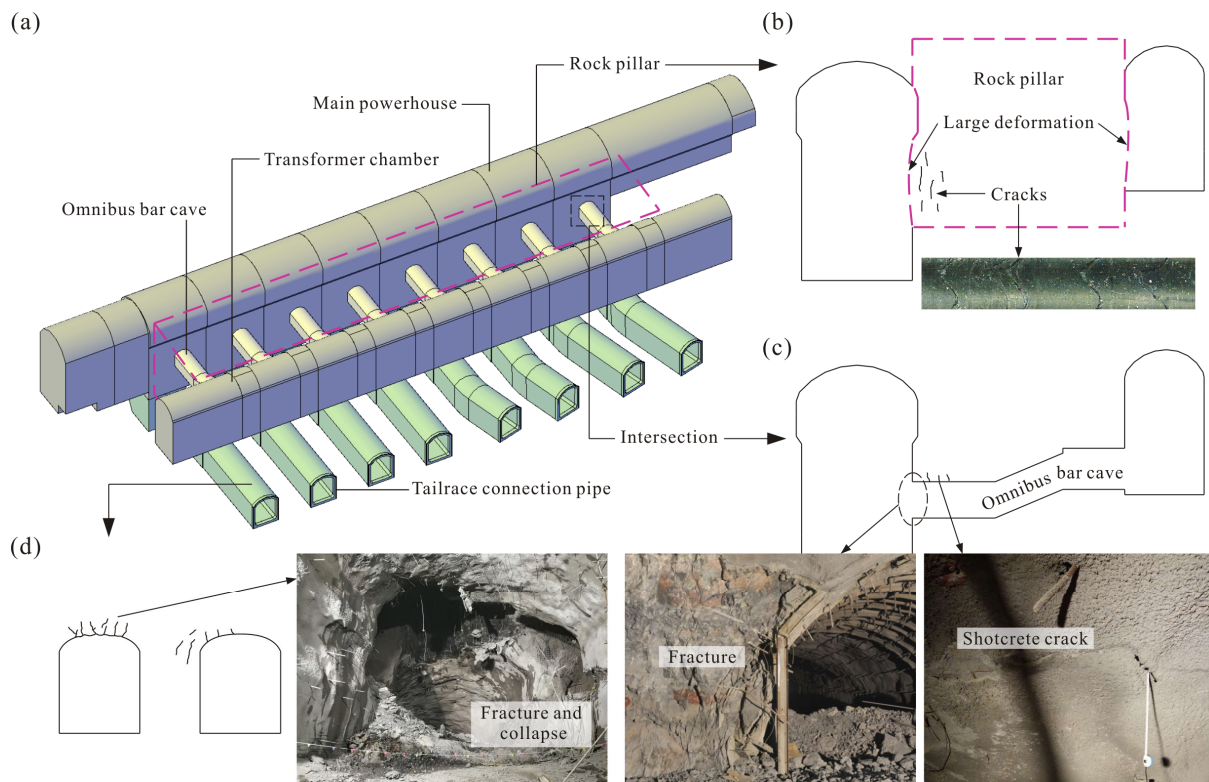


Figure 1. Deformation and failure of surrounding rock mass induced by the multi-cavern effect: (a) a large-scale underground powerhouse, (b) deformation and failure between the main powerhouse and transformer chamber (type LL), (c) between the main powerhouse and omnibus bar cave (type LS) and (d) between tailrace connection pipes (type SS).

The surrounding rock mass failure of the drainage gallery LPL5-1 in the underground powerhouse of the Baihetan hydropower station is a typical case. After excavation and systematic support, the surrounding rock mass of LPL5-1 cracked and failed constantly; this has drawn much attention. The remarkable failure problems in LPL5-1 challenged the surrounding rock mass stability and the builders were worried about the construction and long-term operation safety of the drainage gallery. After failures occurred, builders were eager to find out the cause, evolution, mechanism and countermeasures of failures, and a large number of field investigations and feedback analysis were carried out. It is of significant importance to clarify the failure mechanism for the dynamic adjustment and stability control, which has become a key technical problem restricting the construction of this project due to its uniqueness and complexity. In this paper, the drainage gallery LPL5-1 is considered as a case study. Firstly, by field investigations, the failure characteristics are described. Next, based on numerical simulations, the stress evolution induced by excavation is studied. Then, the correlation between LPL5-1 and the main powerhouse is discussed. Finally, the mechanism of failures is analyzed.

2. Background

2.1. The Baihetan Underground Powerhouse

The Baihetan hydropower station is located on the Jinsha River in southwest China and has the largest underground powerhouse in the world in the mountain on both sides of the river (Figure 2a,b). The left bank underground powerhouse consists of pressure piping, the main powerhouse, omnibus bar caves, a transformer chamber, a draft tube bulkhead gate chamber, tailrace surge chambers and tailrace tunnels (Figure 2c). In addition, the left bank underground powerhouse also includes many auxiliary caverns such as drainage corridors, anchorage observation tunnels, ventilation shafts, access tunnels and construction adits. The main powerhouse is 438 m long and 88.7 m high; its span of 34 m is the largest in the world. The transformer chamber, which is 59.15 m away from the main powerhouse, has a length of 368 m, a span of 21 m and a height of 39.5 m. The span of the draft tube bulkhead gate chamber is 12–15 m, the height is 129.5 m and the length is 374.5 m. The axis of the four tailrace surge chambers is parallel to the main powerhouse and the transformer chamber. The distance between the axis and the centerline of the unit is 220 m and the distance between the axis and the centerline of the transformer chamber is 130.5 m. The diameter of the tailrace surge chambers #1–4 is 44.5–48 m and the height is 124–127.91 m. Generally, the Baihetan underground powerhouse (BUP) features a large-scale and complex structural layout. The main caverns have a large span and high sidewalls. The cavern group has numerous different chambers and tunnels and these caverns are connecting or intersecting with each other. As reflected in Figure 3b, the main powerhouse was excavated in ten layers from May 2014 to June 2018; the transformer chamber was excavated in four layers.

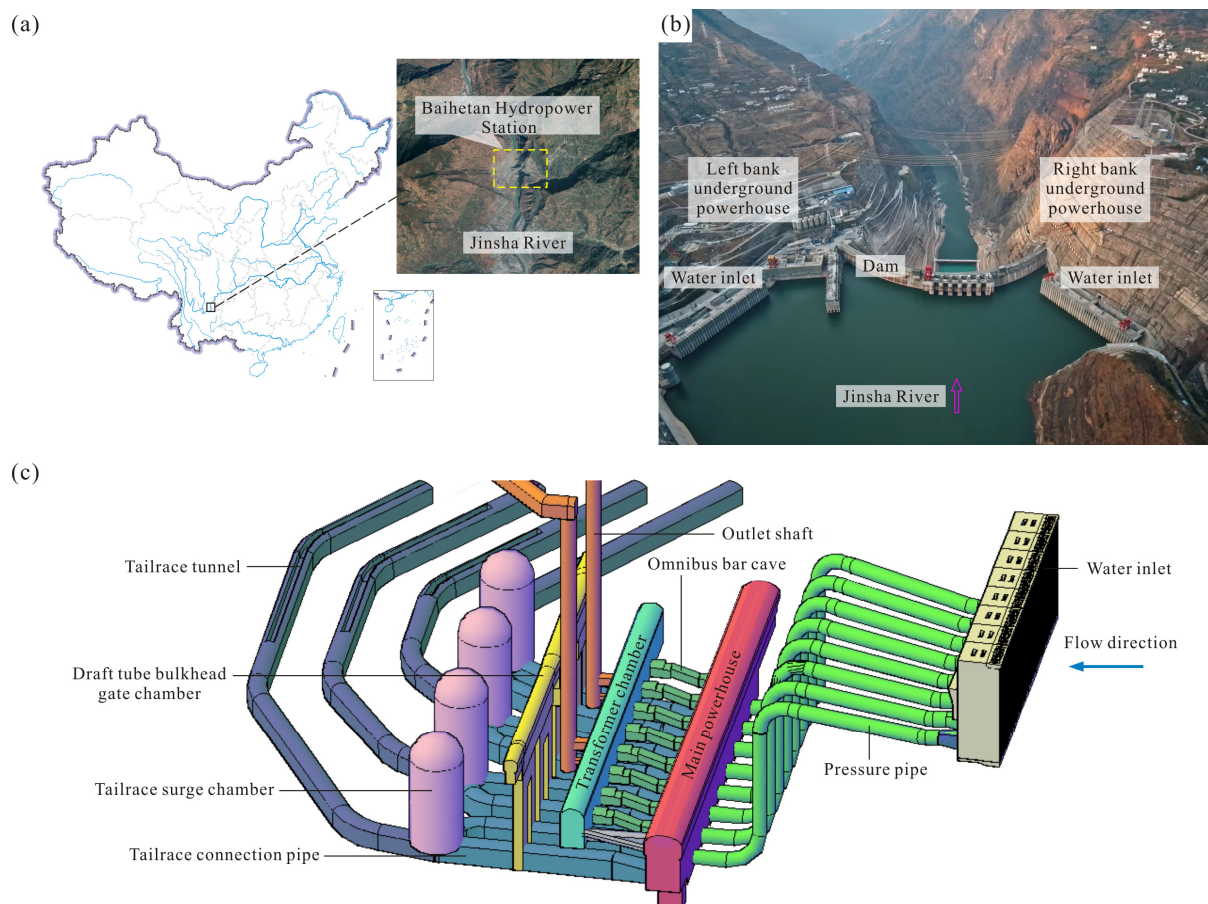


Figure 2. The Baihetan hydropower station and underground powerhouse: (a) the location, (b) an aerial view at the dam site and (c) a three-dimensional layout of the left bank underground powerhouse.

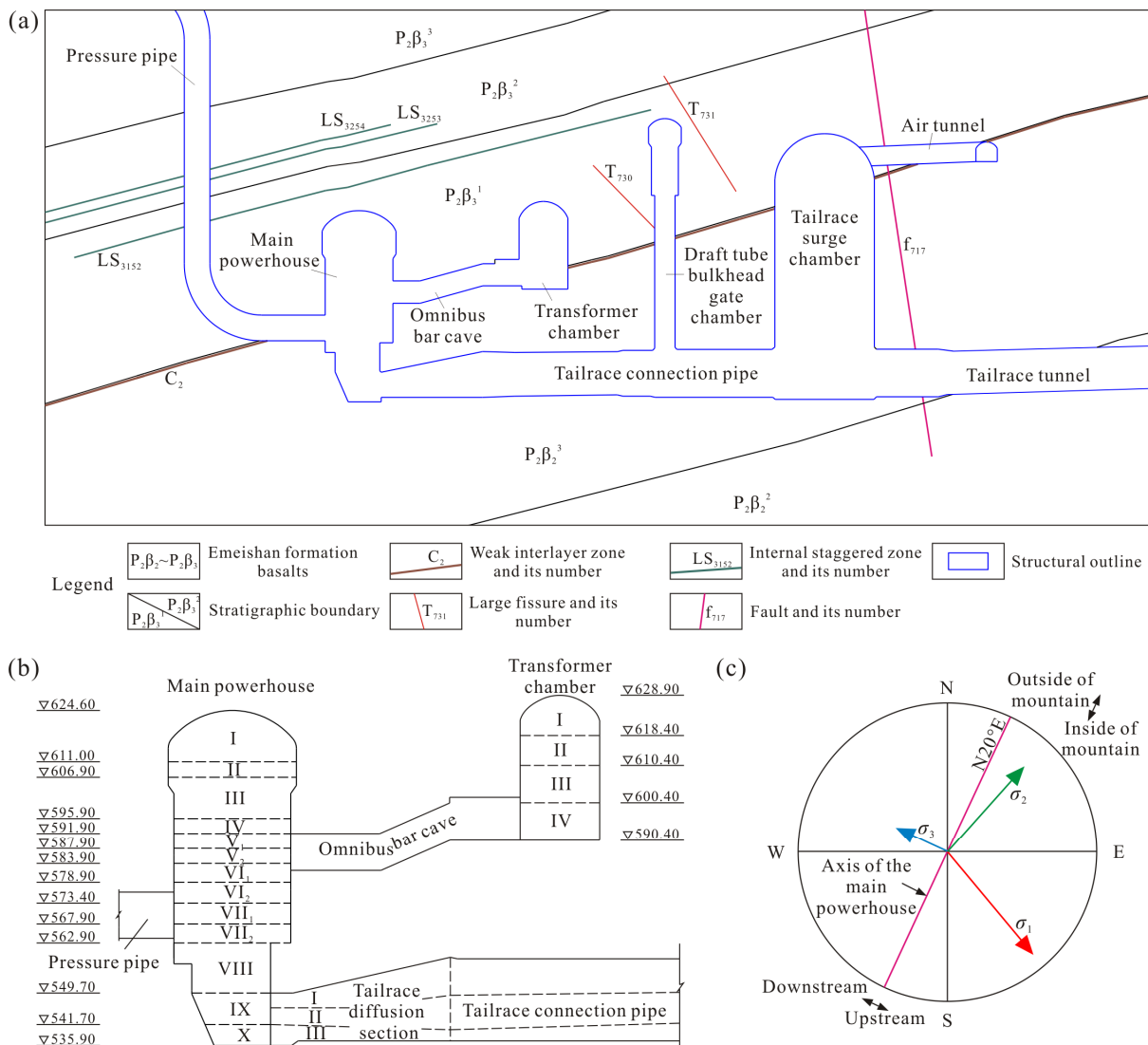


Figure 3. Geological conditions and excavation scheme of the left bank underground powerhouse: (a) a geological cross-section along unit #6, (b) the stratified excavation scheme and (c) the direction of the in situ stress.

2.2. Geological Condition

The underground powerhouse is inside the left bank slope over 300 m high. The horizontal burial depth of the underground powerhouse is 600–1000 m and the vertical burial depth is 260–330 m. The strata surrounding the underground powerhouse are upper Permian Emeishan formation ($P_2\beta$) basalts in monoclinical formations, with strikes of $N40^\circ-45^\circ E$, SE dip directions and dip angles of $15-20^\circ$. From upstream to downstream, the strata are $P_2\beta_4^2, P_2\beta_4^1, P_2\beta_3, P_2\beta_2^4, P_2\beta_2^3$ and $P_2\beta_2^2$ (Figure 3a). The lithology covers aphanitic basalt, oblique tholeiite, amygdaloidal basalt, breccia lava and tuff. The Columnar jointed basalt of three classes is in $P_2\beta_3^2, P_2\beta_3^3$ and $P_2\beta_4^1$. The tuff is in $P_2\beta_3^6, P_2\beta_3^4$ and $P_2\beta_2^4$, with a thickness of 20–80 cm, which is weak and easily softens after absorbing water. The surrounding rock mass is hard and brittle and is mainly subblock structures and local block or mosaic structures. Most of the surrounding rock mass belongs to the III1 category, while some are II or IV.

The geological structures in the underground powerhouse area cover faults, interlayer shear zones, internal shear zones, large fissures and joints. Faults are generally small-scale and rigid structural planes with rock cuttings. Among these faults, the larger ones are F_{13}

and F_{14} , which are exposed in the tailrace tunnels and are 50–200 cm wide. The others are small faults with widths of 5–20 cm. The interlayer shear zone C_2 extends along the middle of the $P_2\beta_2^4$ tuff, with a strike of $N42^\circ-45^\circ E$, a dip direction of SE and a dip angle of $14-17^\circ$. C_2 is 10–60 cm thick and is prone to softening due to its filling of mud and rock cuttings. Internal shear zones cover LS_{3152} and LS_{3253} to LS_{3256} , which are above the top arch of the main powerhouse with a low dip angle. Large fissures are 50–100 m long and share strikes of $N40^\circ-60^\circ W$ and dip angles of $65-85^\circ$; joints have lengths of 2–5 m and widths of less than 1 cm.

2.3. In Situ Stress

Between 2003 and 2011, in situ stress measurements were carried out in the BUP area prior to excavation using the hydraulic fracturing method (HFM) and the stress relief method (SRM). According to the results, the in situ stress is dominated by tectonic stress and, thus, the horizontal stress is larger than the vertical stress. The maximum principal stress is approximately 19–23 MPa, with a strike of $N30^\circ-50^\circ W$ and a dip angle of $5-13^\circ$. The angle between the direction of the maximum principal stress and the axis of the main powerhouse is $50-70^\circ$. The maximum horizontal principal stress reaches 33.39 MPa. The values of the secondary and minimum principal stresses are 13–16 MPa and 8.2–12.2 MPa. The minimum principal stress is almost vertical and its magnitude is equivalent to the gravity stress of the overlying rock mass (Figure 3c). Laboratory test results show that the average saturated compressive strength of the rock in this area is 74–112 MPa, so the strength–stress ratio is 3.22–5.89, which is at a lower level. Overall, the Baihetan left bank underground powerhouse features high in situ stress.

2.4. The Drainage Gallery LPL5-1

The cavern subjected to failure is the drainage gallery LPL5-1. LPL5-1 is located on the upstream side of the main powerhouse, parallel to the powerhouse axis and 28.5 m away from the upstream arch foot, as shown in Figure 4a. The section size of LPL5-1 is $4\text{ m} \times 4\text{ m}$ (width \times height) at stake from ZC0–121.35 m to ZC0–044.2 m and that at stake from ZC0–044.2 m to ZC0+416.15 m is $4\text{ m} \times 5\text{ m}$. LPL5-1 has a length of 537.5 m and a floor elevation of 613–615 m.

Figure 4c presents the geological cross-section of LPL5-1 along the axis. As is reflected, surrounding LPL5-1 is $P_2\beta_3^1$ aphanitic basalt, amygdaloidal basalt, oblique tholeiite, breccia lava and $P_2\beta_3^2$ columnar jointed basalt of the second class, which is hard and brittle. With a strike of $N40^\circ E$, a dip direction of SE and a dip angle of 15° , the strata intersect with the axis of LPL5-1 at an angle of 20° . The geological structures exposed in LPL5-1 are faults, an internal shear zone and joints. Fault f_{717} is filled with brecciated tectonite and is 1–3 cm wide. With a strike of $N55^\circ W$, a dip direction of NE and a dip angle of $80-87^\circ$, f_{717} intersects with the axis of LPL5-1 at a large angle. Internal shear zone LS_{3152} is filled with jointed tectonite and brecciated tectonite, with a strike of $N75^\circ E$, a dip direction of SE and a dip angle of 18° . There are two main joint strikes: $N55^\circ W$ with steep dip angles and $N45^\circ-55^\circ E$ with gentle dip angles. The spacing of joints is generally 50–150 cm and 10–30 cm locally and the surface is closed or filled with a few calcite grains. LPL5-1 is 260–330 m below ground level and is situated in a high in situ stress area. During the excavation of LPL5-1, spalling occurred at the upstream arch (Figure 4b). The surrounding rock mass is dry and no water inflow has been found [15].

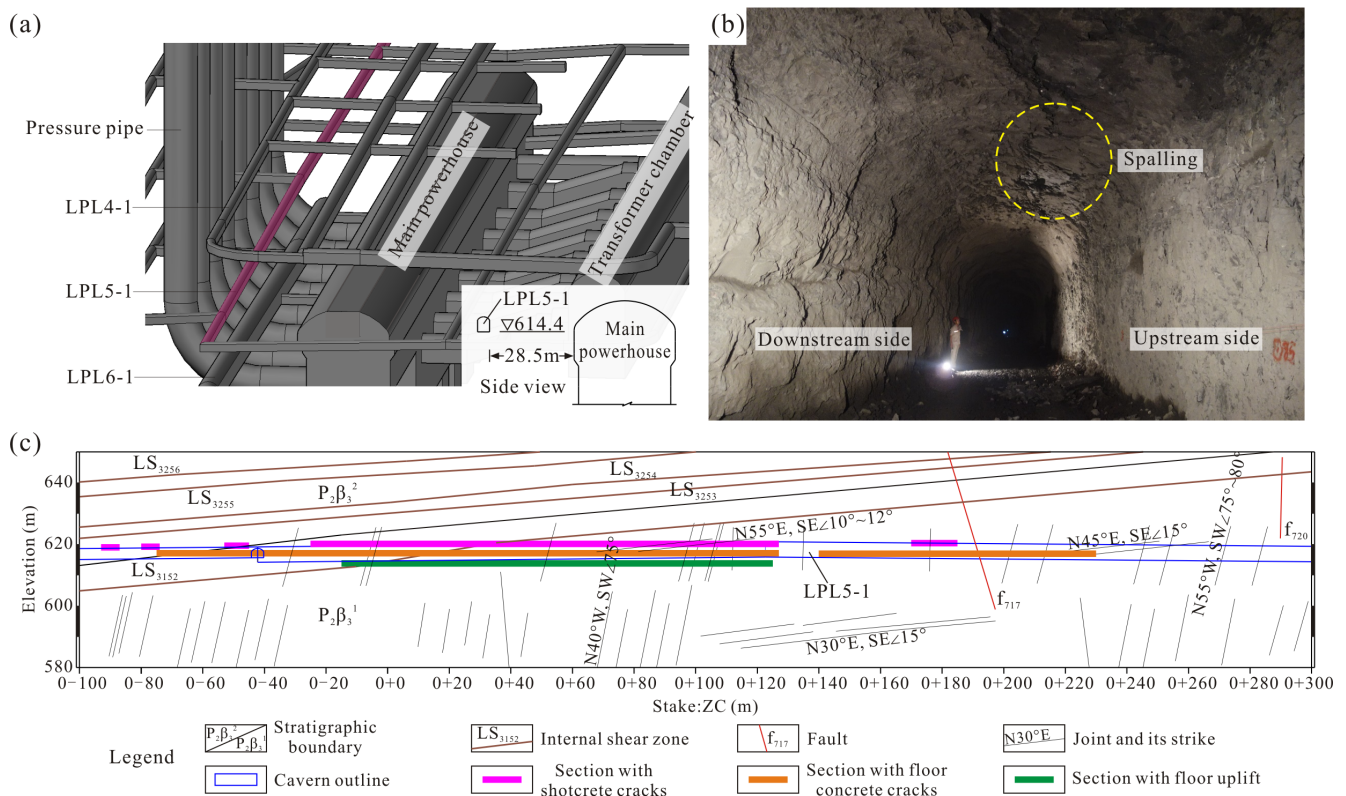


Figure 4. Basic information about the drainage gallery LPL5-1: (a) location, (b) spalling at the upstream arch during excavation and (c) a geological cross-section along the axis and the final axial distribution of failures.

3. Failure Characteristics and Numerical Analysis

3.1. Failure Characteristics

LPL5-1 was excavated and supported by June 2015 when the main powerhouse was excavated at layer II. From then until November 2016, when the excavation of the main powerhouse was at layer III-V, cracks and peeling of shotcrete were found on the upstream arch of LPL5-1 at stake from ZC0–080 m to ZC0+250 m. Cracks extended discontinuously, with a total length of 80 m, accounting for 15% of the LPL5-1 length. To address this problem, reinforcement measures were taken covering supplementary bolts, reinforcement mesh and re-shotcrete, which were finished in January 2017. At the end of March 2017, the shotcrete in LPL5-1 cracked again. The shotcrete on the upstream arch cracked, ballooned and peeled off (Figure 5a). The upstream side floor concrete cracked and swelled, thus separating from the structure below (Figure 5d) [15]. These failures grew with the continuous excavation of the main powerhouse. Shotcrete cracks extended and expanded, shotcrete ballooning evolved into peeling off and the upward displacement of the floor obviously increased (Figure 5f). During the excavation of layers VI₂–VII₁, these failures developed most remarkably. After the main powerhouse was excavated at layer VII₂ in June 2017, the change and development of failures gradually slowed down. Later, in the excavation process of the unit pit, the changing rate decreased significantly. After the excavation of the main powerhouse was completed, there was no apparent change in these failures.

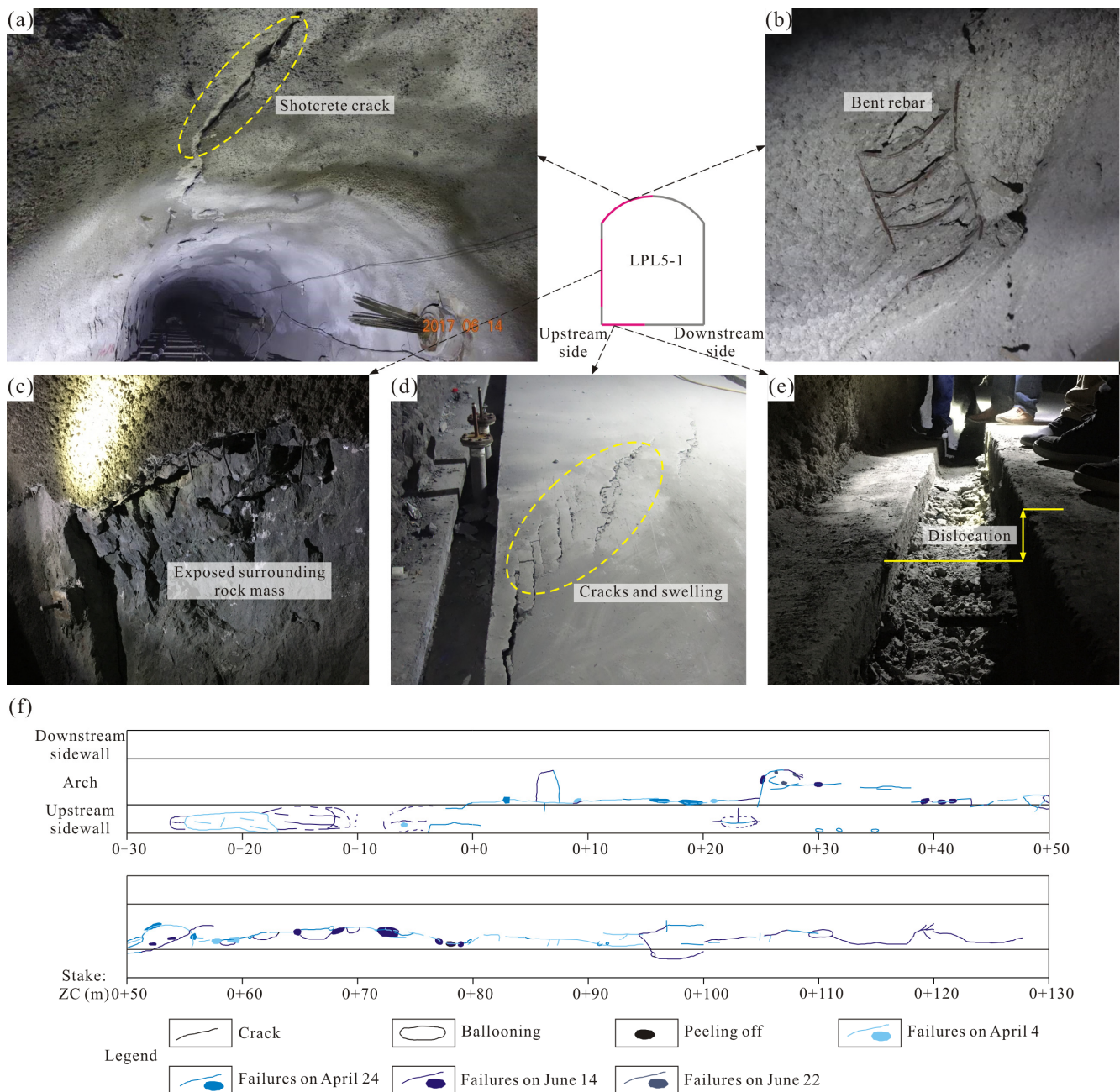


Figure 5. Failures in the drainage gallery LPL5-1: (a) a shotcrete crack and (b) exposed bent rebar at the upstream arch, (c) peeling of shotcrete on the upstream sidewall, (d) cracks and swelling of floor concrete, (e) dislocation on the floor and (f) failure distribution at stake from ZC0–030 m to ZC0+130 m in 2017.

After the excavation was finished, shotcrete failures in LPL5-1 were at stake from ZC0–093 m to ZC0+235 m and the most serious section was from ZC0–026 m to ZC0+130 m. Failures were on the upstream arch, spandrel and sidewall and extended along the axis. The types of failures covered cracks, ballooning and peeling of shotcrete and bending of rebar, as shown in Figure 5a–c. Figure 5d presents cracks on the upstream side floor concrete. At stake from ZC0–15 m to ZC0+125 m, the floor concrete uplifted and separated from the structure beneath. Consequently, cracks, bumps and dislocations arose on the floor, as reflected in Figure 5e. The final distribution of failures in LPL5-1 along the axis is demonstrated in Figure 4c.

3.2. Field Investigation

The failures of the shotcrete and the floor concrete in LPL5-1 aroused considerable attention from the builders. To determine the cause of failure, a field investigation was carried out by means of drilling and geophysical prospecting. Along the axis of LPL5-1, four survey sections were selected and boreholes were drilled on the upstream sidewall, the upstream spandrel and the downstream sidewall, as shown in Figure 6a. Ten boreholes were arranged with depths of 17.45–19.33 m, in which acoustic wave tests and digital camera observations were conducted.

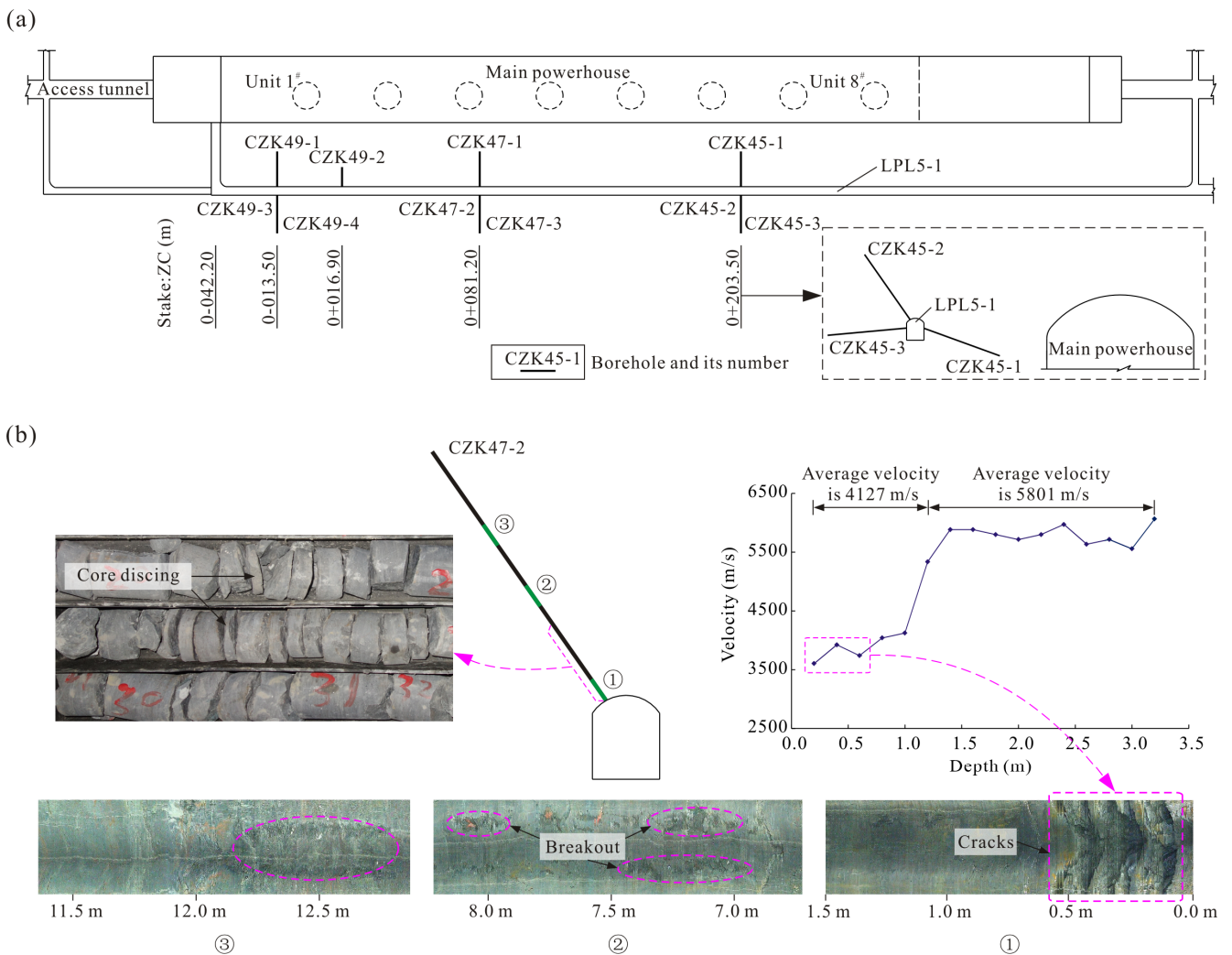


Figure 6. Field investigation and results: (a) layout of survey sections and boreholes from top view and axial view and (b) digital borehole camera images, cores and acoustic wave velocity curve at the upstream spandrel of drainage gallery LPL5-1.

Via the digital borehole camera technique, the dynamic response of the surrounding rock mass during the construction phase can be clearly observed, such as the initiation, propagation and accumulation of cracks in the rock mass. The acoustic wave test can be employed to assess the quality of the surrounding rock mass. With the combined application of these two techniques, the degree of damage and the range of excavation damage zones in the surrounding rock mass can be identified. Figure 6b presents the borehole camera image and the acoustic wave test result of CZK47-2 at the upstream spandrel of section ZC0+81.2 m. The image shows that the rock mass cracked within a depth of 0.6 m and that cracks were distributed densely and were approximately parallel to the free face. These dense cracks indicated that the surrounding rock mass in this range

was damaged. According to the results of the acoustic wave test, the average acoustic wave velocity in the rock mass within a depth of 0.6 m was 3755 m/s, which was the lowest level in CZK47-2. The cracks and damage in the surrounding rock mass accounted for the low wave velocity in this range. In general, the wave velocity curve of CZK47-2 appeared as a step shape. The wave velocity within a depth of 1.2 m was lower, while that at depths over 1.2 m was higher. Thus, we could determine that the range of the excavation damage zone (EDZ) at the upstream spandrel in this section was within a depth of 1.2 m. The surrounding rock mass in the EDZ obviously cracked, while that beyond the EDZ was relatively intact.

The borehole camera image of CZK47-2 showed that breakout, a typical high in situ stress failure, appeared at depths of 7.0–8.2 m and 11.2–11.9 m. Another phenomenon related to high in situ stress, core discing, also occurred in CZK47-2. Conversely, there was no core discing on the downstream side. Breakout and core discing in CZK47-2 proved the high stress around the upstream arch of LPL5-1. Based on the results of field investigation, preliminary conclusions can be drawn as follows:

- (1) The section size of LPL5-1 was relatively small. The surrounding rock mass was hard and most of the rocks were classified as category III. The in situ maximum principal stress was 19–23 MPa. Given all this, only mild spalling would have taken place after excavation. By virtue of systematic support, the surrounding rock mass could have remained stable. The continuous cracking of shotcrete may not be caused by the excavation of LPL5-1; it was possibly related to the stress adjustment induced by the main powerhouse excavation.
- (2) High stress was proven to exist at the upstream arch by core discing and breakouts there. This conclusion agreed with the fact that only the upstream side of LPL5-1 suffered shotcrete failures.
- (3) The floor concrete failure was basically on the surface layer, while the underside concrete did not encounter failure. This result suggested that the floor concrete failure was a result of the uplift and squeezing of the floor, together with the low bond strength between the floor concrete and the underside part.

3.3. Numerical Simulation

The surrounding rock mass failure in LPL5-1 had obvious stress-dominated characteristics. To study the excavation-induced stress evolution in the surrounding rock mass, a numerical simulation of the underground powerhouse excavation was conducted using ANSYS.

The numerical model includes the left bank underground powerhouse and surrounding rock mass, with faults and internal and interlayer shear zones also generated (Figure 7). The dimensions of the model are 600 m × 600 m × 600 m (in the axial, water flow and vertical directions). The element type used in the model is hexahedron SOLID185. The model contains 742,701 nodes and 1,487,340 elements. In general, the range of the model should cover main caverns and geological structures; meanwhile, the dimension of elements should take into account computational accuracy and efficiency. Thus, the model adopts the aforementioned dimension setting. The mesh size is smaller near the periphery of cavern and away from the cavern it is larger. The in situ stress field is simulated by inverse analysis based on field measurement results. According to the stratified excavation scheme, the simulation of excavation is carried out in layers. The constitutive model employed in the calculation is the Mohr–Coulomb model; the mechanical properties adopted are listed in Table 1.

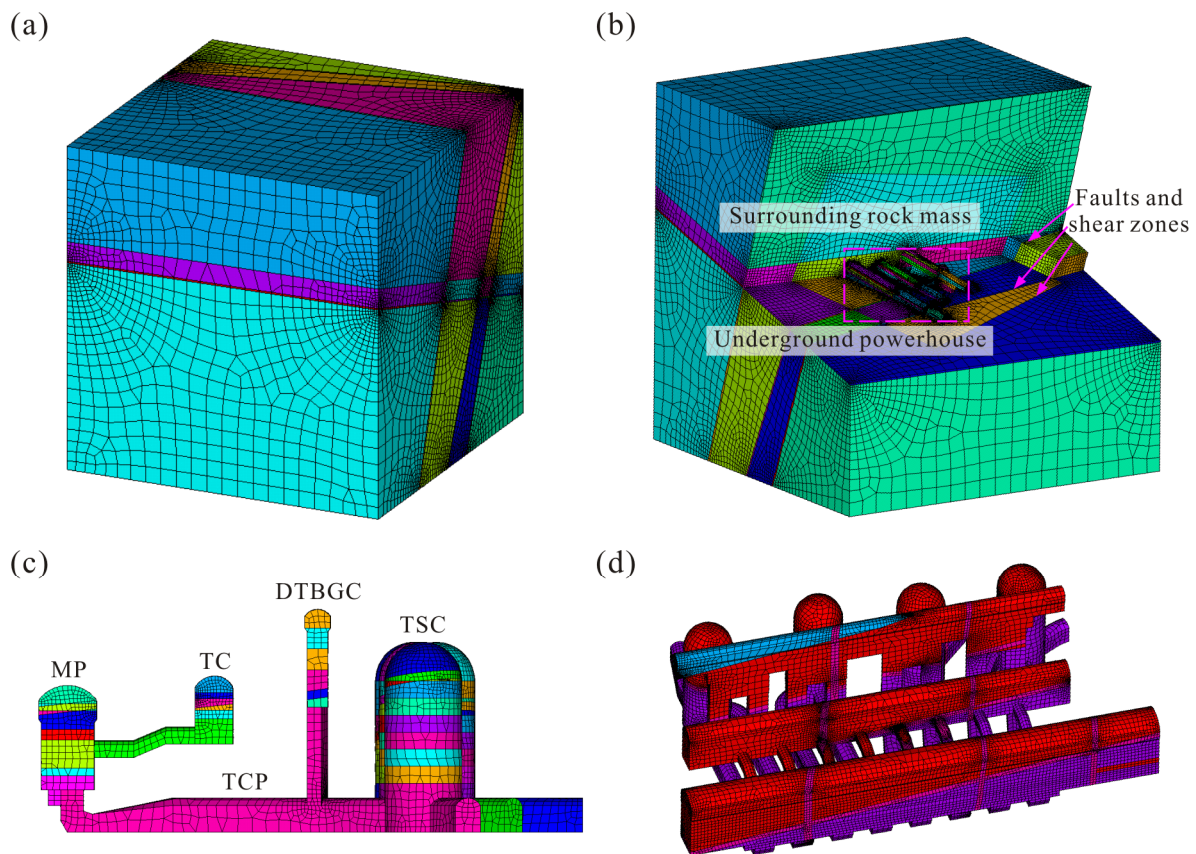


Figure 7. Numerical model: (a) outside of the model, (b) main components of the model, (c) a side view of the underground powerhouse and (d) a three-dimensional diagram of the underground powerhouse. MP, TC, DTBGC, TSC and TCP are abbreviations for the main powerhouse, transformer chamber, draft tube bulkhead gate chamber, tailrace surge chamber and tailrace connection pipe, respectively.

Table 1. Mechanical parameters of the surrounding rock masses used for the numerical simulation.

| Materials | Parameters | Values |
|-----------------------|------------------------------|----------|
| Intact rock | Elasticity modulus (GPa) | 5–19 |
| | Poisson’s ratio | 0.25 |
| | Friction angle | 1.2 |
| | Cohesion (MPa) | 10 |
| | Density (g/cm ³) | 2.7 |
| Interlayer shear zone | Deformation modulus (GPa) | 0.25–0.3 |
| | Friction angle | 0.46–0.5 |
| | Cohesion (MPa) | 0.1–0.17 |
| Internal shear zones | Deformation modulus (GPa) | 0.15–0.3 |
| | Friction angle | 0.36–0.5 |
| | Cohesion (MPa) | 0.05–0.1 |
| Faults | Deformation modulus (GPa) | 0.15–0.3 |
| | Friction angle | 0.36–0.5 |
| | Cohesion (MPa) | 0.05–0.1 |

After the model is established, it is verified. The simulated magnitude of in situ stress is consistent with the measured value. During the simulated excavation of layer I, compressive stress is concentrated at the upstream spandrel of the main powerhouse, which is consistent with the location of the spalling on site. Moreover, the calculated magnitude of the surrounding rock mass deformation is in general accord with the monitoring results.

These agreements prove that the numerical model is valid and the simulation results are reliable.

The simulation results indicate that the surrounding rock mass stress is adjusted and redistributed during excavation, with the radial stress unloading and the tangential stress increasing near free face. Since the direction of the in situ maximum principal stress intersects with the axis of the main powerhouse at a large angle and slightly inclines to the upstream side, a stress concentration zone (SCZ) is generated at the upstream arch of the main powerhouse. As shown in Figure 8a, after the excavation of layer I, the maximum principal stress in the SCZ is 38–44 MPa, which exceeds the crack initiation stress of the Baihetan basalt (34 MPa) [16]. Accordingly, stress-dominated surrounding rock mass failures occur near the free face, such as spalling and splitting. As the stratified excavation is progressed, the stress concentration is intensified and the SCZ scope expands. After the excavation of layer III, the compressive stress at the upstream spandrel is 43–50 MPa and the maximum depth of 34 MPa is about 10 m (Figure 8b). The increased compressive stress can cause the shallow surrounding rock mass split and the shotcrete crack at the upstream spandrel during sidewall excavation. After the excavation of layers IV, V, VI and VII, the maximum depths of 34 MPa are 13 m, 18 m, 20 m and 21.3 m, respectively (Figure 8c–f). The SCZ scope expands with a trend towards the deep and upstream. Under these circumstances, the adjacent caverns, such as LPL5-1, are likely to be affected by stress concentration and subjected to high stress.

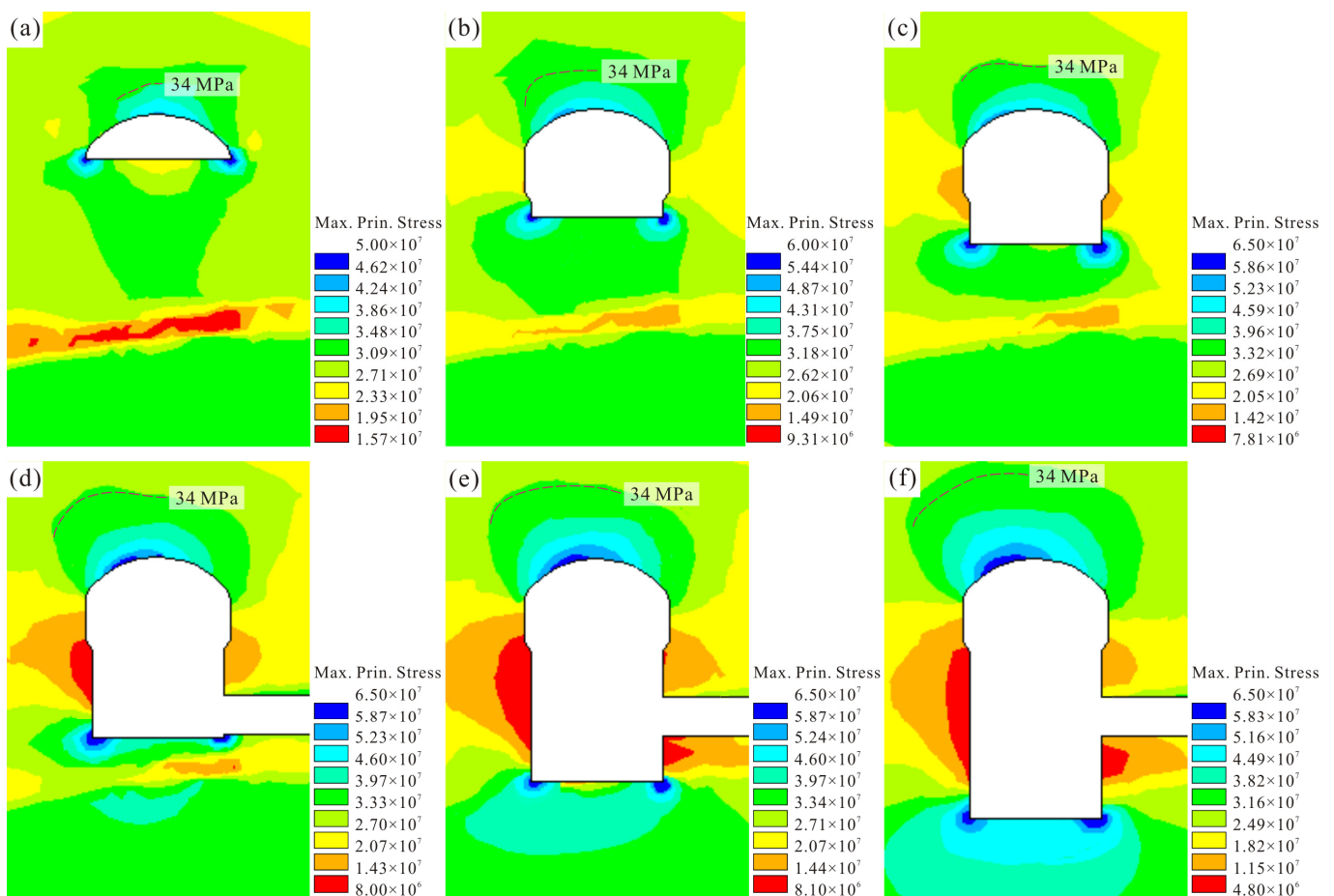


Figure 8. Numerical simulation results: the maximum principal stress distribution in surrounding rock mass during the excavation of (a) layer I, (b) III, (c) IV, (d) V, (e) VI and (f) VII (unit: Pa).

4. Mechanism Analysis

LPL5-1 is situated in relatively good geological condition. The surrounding rock mass is hard and relatively intact and there is no geological structure that can threaten the surrounding rock mass stability. Judging from the failure pattern and location, shotcrete and floor concrete failures in LPL5-1 belong to the stress-dominated type; the geological structure is not a major affecting factor. The in situ maximum principal stress here is 19–23 MPa. When LPL5-1 was excavated, only mild spalling occurred and the surrounding rock mass could have remained stable after systematic support. Why did the failures develop continuously after support? The failures are likely to derive from other nearby caverns, not from LPL5-1 itself.

As reflected in Figure 4a, the caverns around LPL5-1 are LPL4-1, LPL6-1, pressure piping and the main powerhouse. LPL4-1 is above LPL5-1 and has similar excavation dimensions to LPL5-1. The distance between LPL4-1 and LPL5-1 is over 30 m, which exceeds five times the section radius, and the stress adjustment by LPL4-1 excavation was unlikely to have so wide a range that LPL5-1 could be affected. LPL6-1 is also far away and the excavation disturbance has difficulty influencing LPL5-1. The pressure piping is at the upstream side of LPL5-1 and is 20 m away from it, with a section size larger than that of the drainage gallery. However, it is improbable that the pressure piping excavation brought about the failures in LPL5-1. The reason for this inference is as follows.

As shown in Figure 9, the pressure piping is also at the upstream side of LPL6-1, with a distance of 20 m. At the lower horizontal section, the vertical distance between the top arch of pressure piping and the floor of LPL6-1 is about 15 m. LPL6-1 is adjacent to the pressure piping at the upstream and lower side and has a smaller distance than LPL5-1. Hence LPL6-1 is closer to the pressure piping than LPL5-1. Generally, the interaction with respect to rock mass behavior caused by cavern excavation and stress adjustment occurs between adjacent or intersecting caverns and the interaction becomes more significant if the caverns are closer. This has been proven in engineering practice and numerical simulations. If the excavation of pressure piping had an impact on the adjacent caverns, the most obviously affected cavern was LPL6-1. Namely, LPL6-1 should have encountered more serious surrounding rock mass and shotcrete failures than LPL4-1 and LPL5-1. The justification is that the stress adjustment induced by pressure piping excavation will first affect a closer cavern. However, the actual severity of shotcrete cracking in LPL6-1 is much lower than that in LPL5-1. Therefore, the pressure piping excavation is not the controlling factor for the failures in LPL5-1.

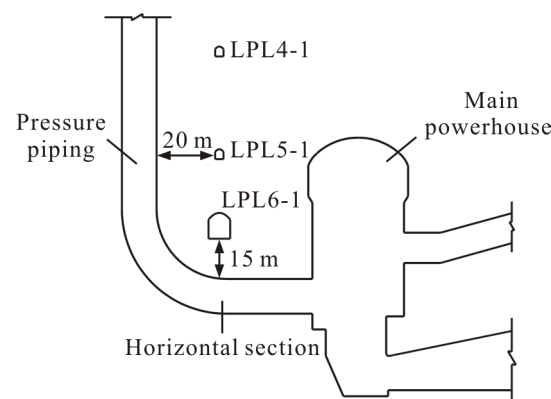


Figure 9. A cross-section of the underground powerhouse.

The main powerhouse is 28.5 m apart from LPL5-1. Although the distance is also large, the stress adjustment from the main powerhouse excavation has a large range due to the large dimensions and long-lasting excavation. So LPL5-1 can be affected by it. For other large caverns, the longer distance makes it less likely for them to influence LPL5-1.

When the shotcrete in LPL5-1 cracked, the sidewalls of the main powerhouse were excavated. The surrounding rock mass stress was in dynamic adjustment and had the potential for influencing adjacent caverns. In terms of failure evolution, there is a connection between the failure development in LPL5-1 and the excavation progress of the main powerhouse. Hence, we can preliminarily conclude that the failures in LPL5-1 resulted from the stress adjustment induced by the main powerhouse excavation. In the following section, the correlation between the failures in LPL5-1 and the main powerhouse excavation will be deeply analyzed in four aspects: failure pattern, failure time, stress adjustment and failure evolution.

1. Correlation in failure pattern

Failure forms in LPL5-1 cover cracking, ballooning and peeling of shotcrete, as well as rebar bending toward the free face. These phenomena indicate that the surrounding rock mass here was subjected to high tangential stress. Similarly, cracking, ballooning and peeling of shotcrete also occurred at the upstream spandrel of the main powerhouse. In terms of form and characteristics, this shotcrete failure is similar to the failures in LPL5-1. The shotcrete failure is distributed at stake ZC0–71.6 m to ZC0+350 m. Shotcrete cracks concentrate on the upstream side of the arch and extend along the main powerhouse axis, as shown in Figure 10. The total length of cracks is about 390 m, accounting for 86.3% of the total length of powerhouse. The width of cracks is generally 3–6 cm, with a local maximum of 16 cm. Shotcrete cracking occurred during the excavation of layer III to VI2 and the evolution of cracks gradually became less obvious later on. The most serious cracking in LPL5-1 is at stake ZC0–026 m to ZC0+130 m and the shotcrete cracks at this section in the main powerhouse are also dense. The similarities in these aspects suggest that the failures in LPL5-1 and the main powerhouse are likely to be caused by the same trigger, i.e., the high tangential stress near the free face at the upstream arch.

2. Correlation in failure time

With respect to failure time, the failures in LPL5-1 are related to those at the upstream spandrel of the main powerhouse. The shotcrete cracking in LPL5-1 started between June 2015 and April 2016; the shotcrete cracking at the upstream spandrel of the main powerhouse began in May 2015. The failures in the main powerhouse and LPL5-1 are successive in time. LPL5-1 is 28.5 m away from the upstream arch foot of the main powerhouse and it takes some time for the SCZ to expand and transfer from the upstream spandrel to LPL5-1. Therefore, the failures in LPL5-1 occur later than those in the main powerhouse. Furthermore, the failures in LPL5-1 are also related to the excavation of the powerhouse sidewalls, that is, the failures run through the sidewall excavation process. Shotcrete failure in LPL5-1 started when the main powerhouse sidewall was excavated at layers III-IV and it developed continuously as the excavation progressed. When the sidewall excavation finished, the change and the development of failures decelerated remarkably. This indicates that the stress adjustment caused by sidewall excavation affected the failures in LPL5-1 as well as the shotcrete cracking at the upstream spandrel of the main powerhouse.

3. Correlation in stress adjustment

According to the numerical simulation results, SCZ forms at the upstream spandrel during the excavation of the main powerhouse. In the SCZ, the compressive stress is high and leads to surrounding rock mass spalling, splitting and shotcrete cracking [17]. The impact scope of SCZ is large and expands upstream with the excavation progress. As a result, LPL5-1 is affected and subjected to high stress. On the other hand, the stress adjustment caused by the excavation of LPL5-1 generates a SCZ at the upstream arch. Since the in situ maximum principal stress inclines slightly to the upstream side, compressive stress concentration occurs at the upstream arch of the main powerhouse and the corridor-shaped caverns parallel to the powerhouse during excavation. This is confirmed by the numerical simulation results and the field spalling in LPL5-1. The SCZ induced by the excavation of

the main powerhouse, in combination with the SCZ induced by the excavation of LPL5-1, puts the surrounding rock mass at the upstream arch of LPL5-1 under high compressive stress, which provides the prerequisite for the failures here. The field investigation found that there is core discing on the upstream side, while there is none on the downstream side, which proves the higher stress at the upstream arch.

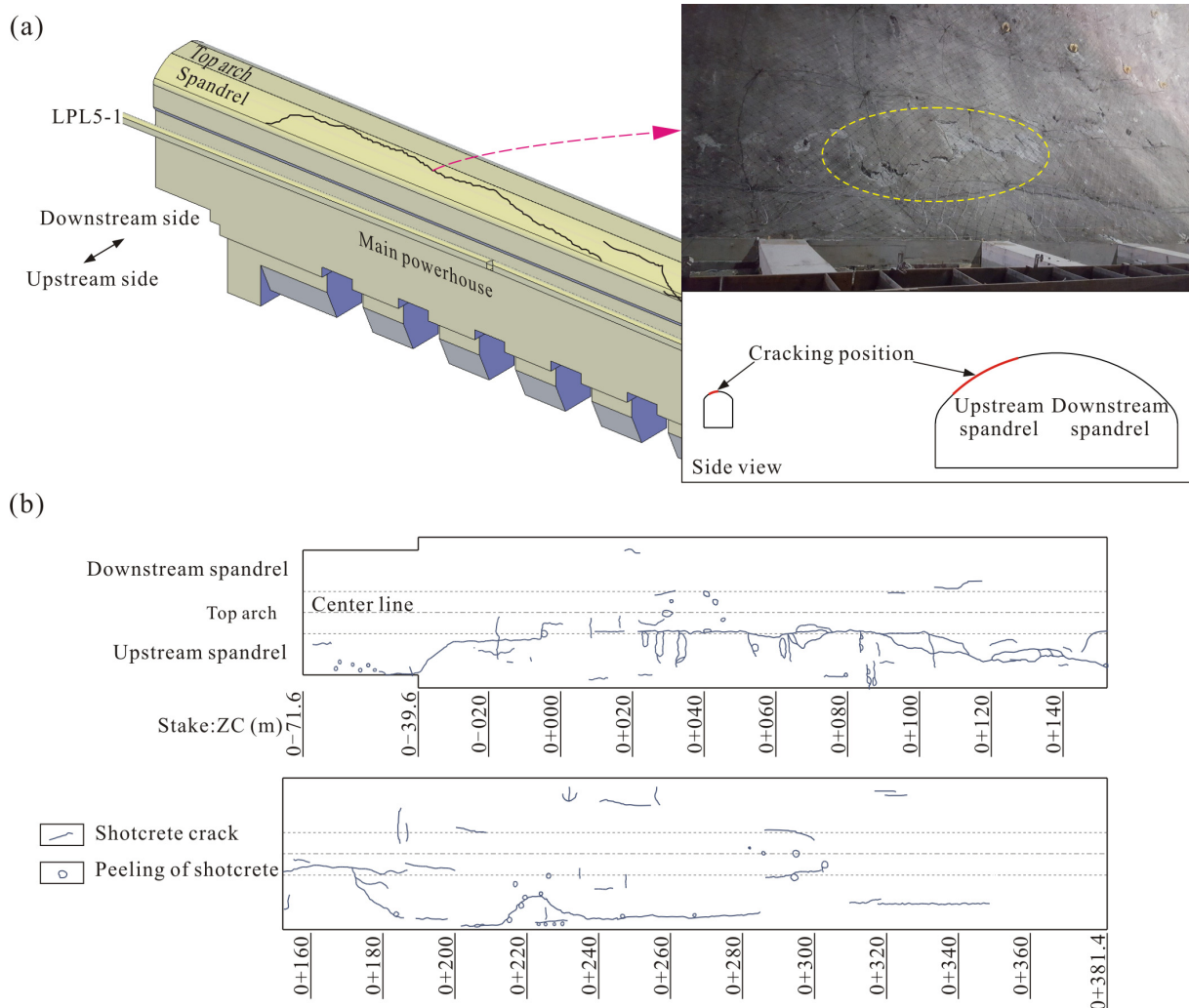


Figure 10. Shotcrete failure at the arch of the main powerhouse: (a) location and photo of shotcrete crack and (b) a distribution diagram of shotcrete failure.

4. Correlation in failure evolution

The extent and evolution of failures in LPL5-1 is closely linked with the excavation progress of the main powerhouse. As the excavation progressed, the failures of shotcrete and floor concrete in LPL5-1 developed. Despite the supplementary reinforced measures, failures occurred again after these measures as the sidewall excavation continued. During the excavation of layer VII₁, when the excavation progress was fast, the failures grew distinctly. Shotcrete cracks extended and expanded and shotcrete ballooning evolved into peeling off. When the excavation was suspended, the development of failures was not apparent. After the main powerhouse excavation was completed, there was no visible change in these failures. These correlations prove once again that the stress adjustment caused by the main powerhouse excavation is the controlling factor of the failures in LPL5-1.

Based on the above analysis, we can conclude that the failures in the drainage gallery LPL5-1 resulted from the expansion of the SCZ at the upstream arch to the upstream

side caused by the main powerhouse excavation. During the excavation of layer I, a SCZ emerged at the upstream arch of the main powerhouse and the high tangential stress σ_t in SCZ resulted in spalling and cracking of the shallow surrounding rock mass. As the excavation progressed continuously, the stress concentration was intensified and the SCZ expanded to the upstream side (Figure 11a). At the upstream spandrel, the surrounding rock mass was split and bent toward the free face, leading to the cracking and ballooning of shotcrete. When the excavation was at layer III, the impact scope of SCZ expanded to LPL5-1, thus putting LPL5-1 under high stress (Figure 11b). Together with the possible stress concentration induced by the LPL5-1 excavation, high σ_t was generated at the upstream arch of LPL5-1. Subjected to the high σ_t , the shallow surrounding rock mass was split (Figure 11c); thus, the failure mechanism of the surrounding rock mass here was splitting failure. Meanwhile, the shallow surrounding rock mass was bent and deformed toward the free face under σ_t . The deformed surrounding rock mass squeezed the shotcrete, which was similar to the condition at the upstream spandrel of the main powerhouse. As a result, the squeezed shotcrete bulged, cracked and evolved to peel off and the rebar was bent. On the upstream floor, the surrounding rock mass was squeezed by the redistributed maximum principal stress and swelled up. Consequently, the floor concrete bulged, cracked and dislocated (Figure 11c). In effect, the failures of the shotcrete and the floor concrete reflect the deformation, splitting and bending failure of the surrounding rock mass. The reason for the failures in LPL5-1 was the multi-cavern effect. The continuous excavation of the main powerhouse exerted an impact on the adjacent LPL5-1, which led to the surrounding rock mass failure in the latter.

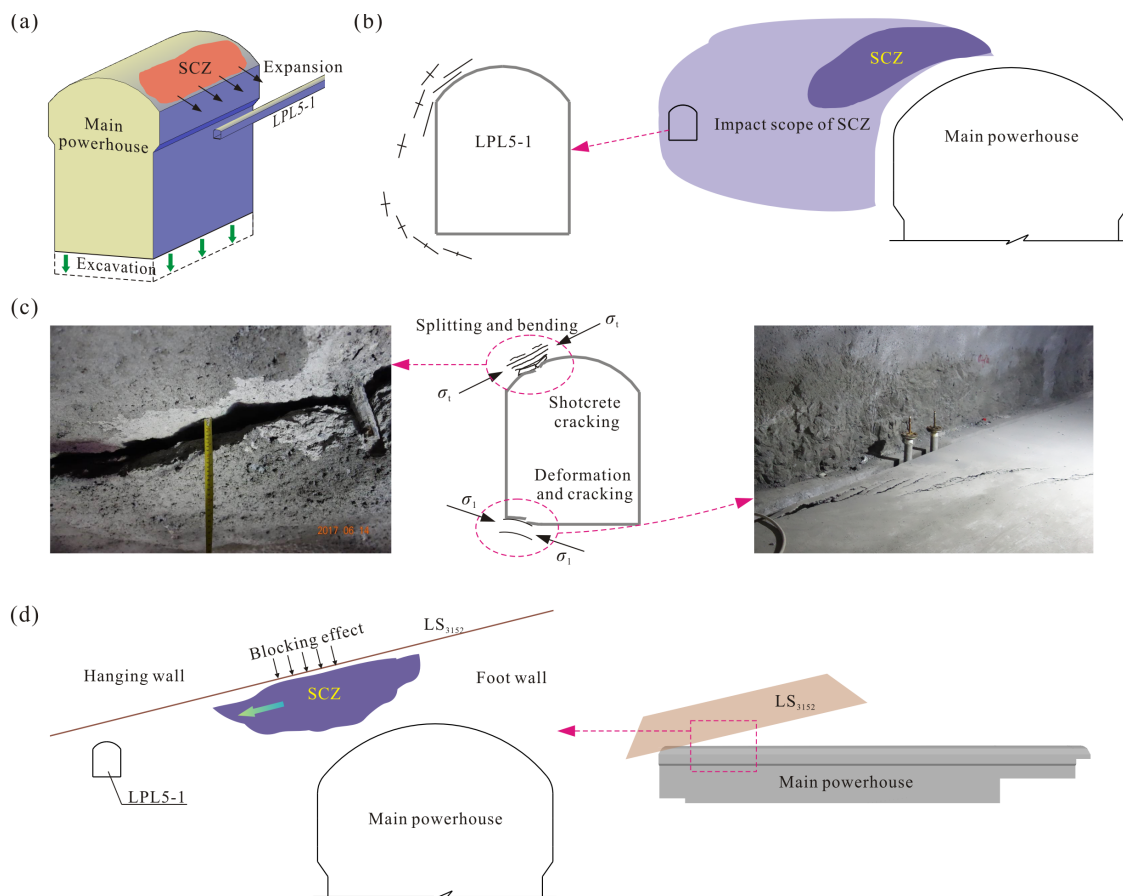


Figure 11. Failure mechanism in the drainage gallery LPL5-1: (a) stress evolution induced by the excavation of the main powerhouse, (b) stress distribution in surrounding rock mass, (c) mechanism of shotcrete and floor concrete cracking in LPL5-1 and (d) stress adjustment under the influence of the internal shear zone.

Moreover, the gently inclined internal shear zone may affect the expansion of SCZ around the main powerhouse. The surrounding rock mass at the upstream top arch and spandrel is cut by internal shear zones such as LS₃₁₅₂. Due to its weakness and discontinuity, the internal shear zone may block the redistributed stress from transferring to the hanging wall [18]. Thus, the stress transfers to both sides of the footwall and the SCZ tends to expand upstream, as reflected in Figure 11d.

5. Discussion

The drainage gallery LPL5-1 is an auxiliary cavern located at the upstream side of the main powerhouse and is 28.5 m away from the upstream arch foot. During the main powerhouse excavation, failures took place at the upstream arch of LPL5-1 covering cracking, ballooning and peeling of shotcrete and rebar bending. These failures reflect the deformation and failure of the surrounding rock mass. To find out the cause of failures, field investigation and numerical simulation are conducted. Based on the results, the reason for failures is the multi-cavern effect. The excavation and stress adjustment of the main powerhouse affects the adjacent LPL5-1, makes it subjected to high redistributed stress and leads to the surrounding rock mass failure.

For a large-scale underground powerhouse, the multi-cavern effect is an issue that cannot be ignored. The multi-cavern effect can arise between large caverns and small caverns, such as the case in this study, or between large caverns, such as the main powerhouse and the transformer chamber. The main powerhouse and the transformer chamber both have a large span and high sidewalls and are usually excavated simultaneously. If the two caverns are too close, each excavation will affect the other and the rock pillar between them is prone to deformation and failure. The rock pillar has two free faces and is unloaded in two directions. The cracking, deformation and the progressive expansion of EDZ induced by excavation and unloading will occur on both sides of the rock pillar. The results of laboratory tests and field observations suggest that the cracks are denser in the shallow rock mass and a few are distributed in the deep rock mass [19]. If the rock pillar is thin, unloading-induced cracking is more liable to affect the other side, thus making EDZ expand or even connect with each other. This synergy or superposition of adjacent excavations that leads to the deformation and failure of the rock pillar is the multi-cavern effect. Compared with the excavation of a single cavern, this multi-cavern effect under bidirectional unloading can trigger more serious deformation and failure.

A large deformation of rock pillar caused by the multi-cavern effect occurred in the Houziyan underground powerhouse (HUP). With respect to the engineering structures, both the BUP and the HUP are large-scale underground powerhouses, although the dimensions of BUP are larger. The distance between the main powerhouse and the transformer chamber of HUP is 45 m, about 1.88 times the average span of the two caverns, while the multiple of BUP is 2.15. Thus, it can be considered that these two caverns of BUP are further apart than those of HUP. In terms of geological conditions, both BUP and HUP are subjected to high in situ stress and complex geological structures. The maximum principal stress at BUP is 19–23 MPa; at HUP it is 22–36 MPa. Faults, weak interlayer zones (WIZs) and joints are developed in both powerhouse areas [20]. Similar to the surrounding rock mass failure in this study, the deformation and failure of HUP is caused by the excavation and unloading of adjacent caverns and the main failure mode is the stress-dominated type. The difference is that the deformation and failure of HUP occurs between two large caverns and the excavation of the two caverns influences each other. The deformation and failure of LPL5-1 occurs between a large cavern and a small cavern, with the former affecting the latter to some extent. In addition, since the main powerhouse and the transformer chamber at BUP are relatively far apart, the interaction of excavation is mitigated. Thus, the rock pillar at BUP did not encounter deformation and failure induced by the multi-cavern effect that HUP experienced.

Furthermore, the multi-cavern effect may also occur between intersecting caverns in the underground powerhouse, such as the omnibus bar cave that intersects with the

powerhouse sidewall belonging to type LS. Zhao et al. [21] studied the failure of rock mass with a WIZ surrounding the intersection of the main powerhouse, the omnibus bar cave and the transformer chamber. By in situ MS monitoring, the spatiotemporal evolution of the surrounding rock mass failure during the excavation of these intersecting chambers was demonstrated and the failure mechanism was analyzed. Li et al. [22] studied the circumferential cracking of the surrounding rock mass of the omnibus bar cave. Via numerical simulation, the stress evolution in the surrounding rock mass caused by the excavation of the omnibus bar cave and the main powerhouse was investigated and the cause of cracking was analyzed. Both studies focus on the surrounding rock mass failure at the intersection of caverns, which reflects the multi-cavern effect. Compared with this study, the multi-free face unloading of surrounding rock mass at the intersection is a difference in these two studies. There are multiple caverns of different sizes and directions at the intersection; these caverns influence each other, thus making the stress evolution and rock mass behavior here more complex. On the other hand, the surrounding rock mass failure in LPL5-1 exhibits time dependence and develops continuously with time or excavation processes, which is not shown in these two studies. The reason is that the stress concentration caused by the powerhouse excavation is intensified with the excavation, causing failures to become increasingly serious. A large-scale underground powerhouse has complex structures compared with other underground openings and this kind of surrounding rock mass stability issue between intersecting caverns is also typical.

In transportation tunnels, the interaction between adjacent tunnels during construction has been noticed [23,24]. In the field of hydroelectric underground powerhouses, the interaction between caverns is also recognized. Xiao et al. suggested that the problem of the multi-cavern effect is prominent in the construction process of underground powerhouses due to their great depth, high in-situ stress and complex geologic structures [25]. Zhang et al. stated that adjacent excavations could exert an influence on EDZ distribution characteristics around a large-scale underground powerhouse [26]. Perras and Diederichs held that there was an interaction of the EDZ between adjacent excavations, which was important and should be considered [27]. In previous studies, since the multi-cavern effect is not the key factor causing deformation and failure, the features and mechanism of the multi-cavern effect have not been thoroughly researched and elucidated. In this study, the multi-cavern effect is the main reason for the failures in LPL5-1. Via field investigation and numerical simulation, the failure mechanism of the surrounding rock mass is revealed. In similar large-scale underground powerhouses, especially under high in situ stress, the problem induced by the multi-cavern effect may also occur, to which attention should be paid. In the future, cases on this aspect will be studied, mechanisms will be explicated, and countermeasures in construction and design will be explored.

6. Conclusions

In the underground powerhouse of the Baihetan hydropower station, the drainage gallery LPL5-1 is arranged parallel to the main powerhouse. During the excavation of the main powerhouse sidewalls, surrounding rock mass failure and cracking and ballooning and peeling of shotcrete occurred at the upstream arch of LPL5-1. The results show that the multi-cavern effect induced by the continuous excavation of the main powerhouse led to failures in LPL5-1. Since the direction of the maximum principal stress intersected with the axis of the main powerhouse at a large angle and inclined slightly to the upstream side, a stress concentration zone was generated at the upstream arch of the main powerhouse. With the continuous excavation of sidewalls and stress adjustment, the stress concentration zone expanded upstream and made LPL5-1 subjected to high stress. Under such an adverse stress state, the shallow surrounding rock mass here was split and bent toward the free face. It squeezed the shotcrete and caused it to crack. The surrounding rock mass on the upstream floor was squeezed and swelled up, causing the floor concrete to crack.

Author Contributions: M.W.: methodology, formal analysis, investigation, writing—original draft and visualization; A.-C.S.: validation, investigation, resources and project administration; H.-B.L.: software, investigation and data curation; H.-C.Y.: software, validation and investigation; G.F.: formal analysis and investigation; J.-W.Z.: conceptualization, writing—review and editing, supervision and funding acquisition. All authors have read and agreed to the published version of the manuscript.

Funding: This research was funded by the Sichuan Youth Science and Technology Innovation Research Team Project, grant number 2020JDTD0006, and the Graduate Student’s Research Innovation Foundation of Sichuan University, grant number 2018YJSY076.

Institutional Review Board Statement: Not applicable.

Informed Consent Statement: Not applicable.

Data Availability Statement: All data that support the findings of this study are available from the corresponding author upon reasonable request.

Acknowledgments: Special thanks are extended to the Hydro China Huadong Engineering Corporation for providing geological information and field data.

Conflicts of Interest: The authors declare no conflict of interest.

References

- Li, B.; Xu, N.W.; Dai, F.; Zhang, G.L.; Xiao, P.W. Dynamic analysis of rock mass deform in large underground caverns considering microseismic data. *Int. J. Rock Mech. Min.* **2019**, *122*, 104078. [[CrossRef](#)]
- Liu, W.R.; Xu, J.; Wang, Z.; Peng, C. Experimental research on damage characteristics and safety damage threshold of jointed caverns based on acoustic emissions. *Geomech. Geophys. Geo.* **2021**, *7*, 72. [[CrossRef](#)]
- Ding, X.L.; Niu, X.Q.; Pei, Q.T.; Huang, S.L.; Zhang, Y.T.; Zhang, C.H. Stability of large underground caverns excavated in layered rock masses with steep dip angles: A case study. *Bull. Eng. Geol. Environ.* **2019**, *78*, 5101–5133. [[CrossRef](#)]
- Zhou, Y.Y.; Xu, D.P.; Gu, G.K.; Liu, K.; Wan, L.P.; Wang, T.L.; Yang, J.B. The failure mechanism and construction practice of large underground caverns in steeply dipping layered rock masses. *Eng. Geol.* **2019**, *50*, 45–64. [[CrossRef](#)]
- Xiao, Y.X.; Feng, X.T.; Feng, G.L.; Liu, H.J.; Jiang, Q.; Qiu, S.L. Mechanism of evolution of stress-structure controlled collapse of surrounding rock in caverns: A case study from the Baihetan hydropower station in China. *Tunn. Undergr. Space Technol.* **2016**, *51*, 56–67. [[CrossRef](#)]
- Hu, Z.H.; Xu, N.W.; Li, B.; Xu, Y.; Xu, J.; Wang, K. Stability analysis of the arch crown of a large-scale underground powerhouse during excavation. *Rock Mech. Rock Eng.* **2020**, *53*, 2935–2943. [[CrossRef](#)]
- Wang, M.; Zhou, J.W.; Chen, J.L.; Jiang, N.; Zhang, P.W.; Li, H.B. Automatic identification of rock discontinuity and stability analysis of tunnel rock blocks using terrestrial laser scanning. *J. Rock Mech. Geotech. Eng.* **2023**; *in press*. [[CrossRef](#)]
- Liu, F.; Ma, T.H.; Tang, C.A.; Chen, F. Prediction of rockburst in tunnels at the Jinping II hydropower station using microseismic monitoring technique. *Tunn. Undergr. Sp. Tech.* **2018**, *81*, 480–493. [[CrossRef](#)]
- Xue, Y.G.; Li, Z.Q.; Li, S.C.; Qiu, D.H.; Tao, Y.F.; Wang, L.; Yang, W.M.; Zhang, K. Prediction of rock burst in underground caverns based on rough set and extensible comprehensive evaluation. *Bull. Eng. Geol. Environ.* **2019**, *78*, 417–429. [[CrossRef](#)]
- Wang, T.; Fan, B.W.; Khadka, S.S. Flowchart of DEM modeling stability analysis of large underground powerhouse caverns. *Adv. Civ. Eng.* **2020**, *2020*, 8874120. [[CrossRef](#)]
- Kumar, V.; Jha, P.C.; Singh, N.P.; Cherukuri, S. Dynamic stability evaluation of underground powerhouse cavern using microseismic monitoring. *Geotech. Geol. Eng.* **2021**, *39*, 1795–1815. [[CrossRef](#)]
- Li, A.; Dai, F.; Liu, Y.; Du, H.B.; Jiang, R.C. Dynamic stability evaluation of underground cavern sidewalls against flexural toppling considering excavation-induced damage. *Tunn. Undergr. Space Technol.* **2021**, *112*, 103903. [[CrossRef](#)]
- Ren, Q.W.; Xu, L.; Zhu, A.X.; Shan, M.Z.; Zhang, L.F.; Gu, J.F.; Shen, L. Comprehensive safety evaluation method of surrounding rock during underground cavern construction. *Undergr. Space* **2021**, *6*, 46–61. [[CrossRef](#)]
- Zhang, Y.; Su, G.S.; Liu, B.C.; Li, T.B. A novel displacement back analysis method considering the displacement loss for underground rock mass engineering. *Tunn. Undergr. Space Technol.* **2020**, *95*, 1–15. [[CrossRef](#)]
- Hydro China Huadong Engineering Corporation. *Volume I Engineering Geology, Volume II Design Report, Special Acceptance of the Underground Powerhouse of the Baihetan Hydropower Station on the Jinsha River during the Excavation and Support Phase*; PowerChina Huadong Engineering Corporation Limited: Hangzhou, China, 2019.
- Wang, M.; Shi, A.C.; Zhou, J.W.; Fan, G.; Yan, H.C.; Li, H.B. Response characteristic analysis of the deformation and failure of surrounding rock mass in a large underground powerhouse under high in-situ stress. *J. Eng. Geol.* **2021**, *29*, 18–27.
- Shi, A.C.; Li, C.J.; Hong, W.B.; Lu, G.D.; Zhou, J.W.; Li, H.B. Comparative analysis of deformation and failure mechanisms of underground powerhouses on the left and right banks of Baihetan hydropower station. *J. Rock Mech. Geotech. Eng.* **2022**, *14*, 731–745. [[CrossRef](#)]
- Wang, M.; Shi, A.C.; Li, H.B.; Yan, H.C.; Fan, G.; Zhou, J.W. Deformation and failure mechanism analyses for the surrounding rock mass in a large cylindrical tailrace surge chamber. *Arab. J. Geosci.* **2022**, *15*, 400. [[CrossRef](#)]

19. Zhu, W.S.; Yang, W.M.; Xiang, L.; Li, X.J.; Zheng, W.H. Laboratory and field study of splitting failure on side wall of large-scale cavern and feedback analysis. *Chin. J. Rock Mech. Eng.* **2011**, *30*, 1310–1317.
20. Xiao, X.H.; Xiao, P.W.; Dai, F.; Li, H.B.; Zhang, X.B.; Zhou, J.W. Large deformation characteristics and reinforcement measures for a rock pillar in the Houziyan underground powerhouse. *Rock Mech. Rock Eng.* **2017**, *51*, 561–578. [[CrossRef](#)]
21. Zhao, J.S.; Feng, X.T.; Jiang, Q.; Zhou, Y.Y. Microseismicity monitoring and failure mechanism analysis of rock masses with weak interlayer zone in underground intersecting chambers: A case study from the Baihetan Hydropower Station, China. *Eng. Geol.* **2018**, *245*, 44–60. [[CrossRef](#)]
22. Li, N.; Sun, H.C.; Yao, X.C.; Shi, G.B. Cause analysis of circumferential splits in surrounding rock of busbar tunnels in underground powerhouses and reinforced measures. *Chin. J. Rock Mech. Eng.* **2008**, *27*, 439–446.
23. Ng, C.W.W.; Lee, K.M.; Tang, D.K.W. Three-dimensional numerical investigations of new Austrian tunnelling method (NATM) twin tunnel interactions. *Can. Geotech. J.* **2004**, *41*, 523–539. [[CrossRef](#)]
24. Choi, J.I.; Lee, S.W. Influence of existing tunnel on mechanical behavior of new tunnel. *KSCE J. Civ. Eng.* **2010**, *14*, 773–783. [[CrossRef](#)]
25. Xiao, P.W.; Qian, B.; Jiang, P.; Xu, N.W.; Li, B. Deformation forecasting of surrounding rock mass based on correlation between frequency and fracture scale of microseismicity. *Adv. Civ. Eng.* **2018**, *2018*, 4037402. [[CrossRef](#)]
26. Zhang, L.G.; Wang, D.; Dong, J.X. Assessment of the excavation damaged zones in the surrounding rock of an underground powerhouse under high in situ stress using an acoustic velocity detecting method. *Adv. Civ. Eng.* **2020**, *2020*, 7297260. [[CrossRef](#)]
27. Perras, M.A.; Diederichs, M.S. Predicting excavation damage zone depths in brittle rocks. *J. Rock Mech. Geotech. Eng.* **2016**, *8*, 60–74. [[CrossRef](#)]

Disclaimer/Publisher’s Note: The statements, opinions and data contained in all publications are solely those of the individual author(s) and contributor(s) and not of MDPI and/or the editor(s). MDPI and/or the editor(s) disclaim responsibility for any injury to people or property resulting from any ideas, methods, instructions or products referred to in the content.